The pressure effect on the wax formation in diesel fuel☆

Jérôme Pauly[a,*], Jean-Luc Daridon[a], Jean-Marc Sansot[a], J.A.P. Coutinho[b]

[a]High Pressure Laboratory, University of Pau et des Pays de l'Adour, GHP BP 1155, 64013 Pau, France
[b]Departemento de Quimica da Universidade de Aveiro, 3810-193 Aveiro, Portugal

Available online 6 November 2002

Abstract

The prevention of wax formation under high pressure on new diesel engine requires a good understanding of the behaviour of the paraffin molecules crystallization. In this work a diesel from a Petrogal refinery was investigated under pressure. In particular the melting curve was measured from atmospheric pressure to 100 MPa by an optical technique. The behaviour of the solid phase with the pressure was also investigated up to 50 MPa by filtration. The results obtained show an increase in the diesel cloud point of about 25 °C at the operating pressure of a common rail engine. It is clear from our results that the increase of the diesel cloud point must be taken into account in the development of new diesel engines where the diesel is injected under high pressure.

All the results obtained were successfully predicted with a thermodynamic model able to describe multiphase equilibrium.
© 2002 Elsevier Science Ltd. All rights reserved.

Keywords: Wax; Multiphase; Filtration

1. Introduction

The global warming of our planet poses a major threat to the life it supports. In particular the burning of fossil fuels releases CO_2 which entraps the solar radiation near the earth's surface. This is one of the major reasons why the development of innovative engine technology has been a priority for car manufacturers.

For many years the diesel engines have been commonly used in buses, cars and lorries because they have many advantages in comparison with gasoline engines. Their higher efficiency allows less fuel to be used for the same distance leading to less carbon dioxide released. This low fuel consumption as well as their high durability are the main reason for the popularity of diesel engines.

However, diesels have an image of being dirty due to the amount of the black particles emitted to the atmosphere. Aiming at solve this problem the diesel engines are becoming more efficient. Recently a new generation of direct injection systems based on the injection of the fuel under high pressure, known as common rail was born. All the manufacturers are convinced that the high pressure is a solution to reduce drastically the level of pollution of the diesel engine. The pressure in these systems called commonly 'common rail' can reach 130 MPa that is about ten times the pressure in an indirect pressure engine.

It is, therefore, very important to take into account the influence of the pressure in the thermodynamic behaviour of the diesel fuel. The prevention of the wax formation in this hydrocarbon fluids at low temperature and high pressure is necessary to avoid the appearance of a solid fraction responsible for the plugging of diesel filters and connective lines.

To improve the knowledge of the solid formation under pressure, the behaviour of a diesel from a refinery, already investigated at atmospheric temperature [1], is studied here under high pressure. The melting line in a range of pressure going from 0.1 to 100 MPa was measured using an optical technique [2] whereas the evolution of the paraffinic solid phase with the pressure is experimentally assessed on equilibrium cell by a filtration technique [3]. Concurrently these results are described with a predictive thermodynamic model [4]. It is shown that a good representation of the pressure influence on the diesel studied is obtained with the model used.

2. Experimental section

2.1. Wax disappearance temperature apparatus

Several procedures for the measurement of the melting boundaries of pure long-chain *n*-alkanes have been proposed in the literature including acoustic, mechanical, optical visual and calorimetric techniques [5]. It is clear today that most of these approaches become inaccurate when applied to complex mixtures and dark oils. The best and most reliable technique available seems to be the microscopy of transmitted polarized light known as cross polar microscopy. For the purpose of studying complex systems, such as the diesel reported here, an optical apparatus has been designed to determined visually the solid–liquid phase transitions under high pressure using a polarizing micro-scope [2]. The apparatus is made up of a high pressure in which two transparent windows make possible to observe the system under pressure up to 100 MPa with a cross-polarization microscope. Its optical as well as the geometric size of the cell allow the observation of crystals of 2 μm in length in a sample volume of 30 mm^3.

The temperature of the system in the high pressure cell is thermo regulated by the flow of a heat-carrying fluid with a stability of 0.01 K over a temperature range of between 243 and 373 K. The pressure is achieved by a high pressure pneumatic pump connected to a tank in which a mobile piston can move. The pressure probe is placed directly on the circuit with the studied system and is connected to a manometer ensuring an accuracy of 0.02%. To avoid crystallization beyond the optical cell, the tank as well as the tubing are closed in an oven with air circulation keeping its temperature above the melting point of the fluid.

In order to avoid the problem related to the subcooling effects during a phase change between the single liquid phase and the two phases liquid–solid region, the melting point was determined by measuring the disappearance of the last crystal of solid (wax disappearance temperature (WDP)) during a heating process.

2.2. Solid liquid equilibrium filtration apparatus

The characterization of the fluid behaviour below the wax appearance temperature as a function of pressure is obtained by isobaric filtration method through a filter system. The apparatus, which has been described previously in detail [3], is essentially made up of two stainless steel autoclave cylinders separated by a filtration disc of sintered steel of 3 μm porosity and closed at their extremities by pistons which separate the sample studied and the compression oil. The main advantage of the cell is that the first piston can be dismantled making easier the recover of both solid residue and liquid phase. To ensure satisfactory thermal uniformity within the fluid, the cell is fully immersed in a refrigerated thermostat bath which is agitated and thermo-regulated by a thermostat with a stability of

0.02 K. The measurements can be performed up to a maximum pressure of 50 MPa achieved by a twin-body volumetric pump operating with compression oil. This pump is able to impose the pressure on both sides of the filtering system leading to an isobaric transfer of the liquid through the filter. The pressure is measured by two probes placed in the compression oil circuit ensuring a measure-ment accuracy within the sample of 0.05 MPa.

Both liquid phase and solid residue composed by solids and entrapped liquid are analysed by gas chromatography. To assess the real wax content and compositions of the wax, it is necessary to determine the quantities of liquid trapped. A mathematical correction based on the knowledge of both composition of the filtrate and overall composition of diesel investigated is employed as described in a previous work [6].

2.3. Results

The PNA distribution for the diesel investigated here was known from 'carburane' process [7] and was confirmed for the *n*-alkanes distribution by our gas chromatography analysis [1]. This composition as well as the average molecular weight of the PNA distribution is presented in Table 1.

The wax disappearance temperatures were measured with the optical cell from 0.1 to 100 MPa every 20 MPa. The results are reported on Table 2 and presented in Fig. 1. The wax disappearance temperature increases almost linearly with

Table 1
Composition (mass fraction) of the diesel [23]

Components	Diesel mass fraction ($\times 10^3$)
n-C10	1.392
n-C11	1.957
n-C12	4.235
n-C13	9.121
n-C14	10.47
n-C15	12.78
n-C16	10.1
n-C17	9.694
n-C18	8.111
n-C19	7.138
n-C20	6.617
n-C21	5.612
n-C22	4.58
n-C23	3.814
n-C24	3.044
n-C25	2.631
n-C26	1.862
n-C27	1.314
n-C28	0.8502
n-C29	0.6342
n-C30	0.3082
n-C31	0.1921
n-C32	0.1079
Paraffins	0.1066
Naphthenic	0.6717
Aromatic	0.2217
M_w (g/mol)	212.6

Table 2
Wax appearance temperature: experimental data and calculated points

	Pressure (MPa)					
	0.1	20	40	60	80	100
Experimental (K)	280.30	283.65	287.15	290.75	294.25	297.35
Calculated (K)	280.19	283.95	287.44	290.85	293.97	297.20

pressure. If the melting curve is assumed linear the calculation of the slope gives a value of 0.17 °C MPa^{-1} showing that the influence of the pressure cannot be neglected by the car manufacturers. This value is lower than the values obtained for pure alkanes [8–10]. As the injection pressure of the diesel in a 'common rail' engine is about 130 MPa, a 22 °C increase of the diesel cloud point is expected. Two different preventive curative methods can be tested by manufactures: heating the lines or using additives even if they are not sure about their efficiency under high pressure.

The measurements in the equilibrium filtration cell aim at obtaining the composition of the phases in equilibrium and the fraction of solids in the mixture for pressures between 0.1 and 50 MPa at a constant temperature of 263.15 K. The composition of the solid deposit (mass%) as well as the percentage of total paraffins crystallized is given in Table 3. Fig. 2 represents the percentage of total paraffins crystallized in function of the pressure. The results under pressure are in good agreement with results at atmospheric pressure. It is logical to obtain an increase of the total amount of paraffins crystallized while the filtration condition becomes more and more distant of the melting point when the pressure grows. Fig. 3 describes the solid phase evolution with pressure. It denotes a slow appearance of lightest components of the heavy fraction with the pressure increase leading, at high pressures, to an *n*-alkane distribution of the solid phase closed to the distribution in the initial diesel.

3. Modelling

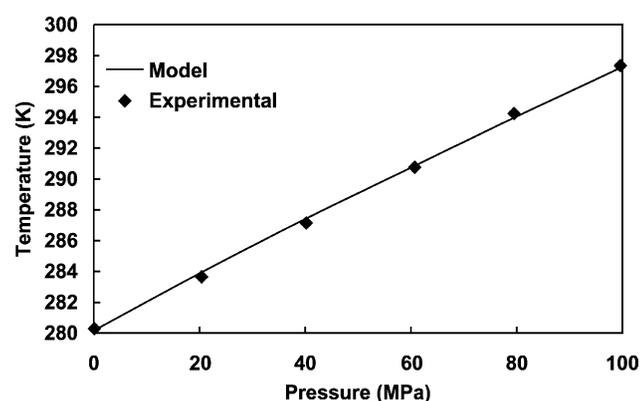Most of the work dealing with wax precipitation modelling are based on wrong hypothesis concerning the

Table 3
Percentage of total paraffins crystallized and composition (mass%) of the solid phase vs pressure at 263.15 K

	P (MPa)				
	0.1[a]	10	20	30	50
% Paraffins crystallized	12.22[a]	16.95	17.9	22.31	27.64
Solid phase composition (%)[a]					
C10	0	0	0	0	0
C11	0	0	0	0	0
C12	0	0	0	0	0
C13	0	0	0	0	0
C14	0	0	0	0	0.338
C15	0	0	0	0	0.63
C16	0	0	0	0.94	1.92
C17	0	0	0.67	1.10	2.35
C18	1.46	1.15	3.14	3.52	5.02
C19	4.47	1.90	3.91	4.83	5.59
C20	9.04	4.01	8.48	8.50	7.75
C21	12.90	8.03	12.80	11.30	10.80
C22	14.80	10.80	14.80	12.40	12.30
C23	13.80	14.00	14.00	11.60	10.90
C24	12.00	15.30	10.00	9.79	10.20
C25	9.74	13.00	9.58	7.99	8.80
C26	7.24	9.31	7.34	6.79	7.27
C27	5.46	6.59	5.71	6.24	5.91
C28	3.33	6.66	3.99	4.67	3.96
C29	2.43	4.47	2.58	3.74	3.24
C30	1.34	3.31	1.46	3.10	1.97
C31	0.78	0.92	0.91	2.06	0.7
C32	0.38	0.57	0.56	1.54	0.41

[a] From Ref. [23].

nature of the solid phases. A first type of model considers the solid phase as a single or multiple pure solid phases [11] whereas a second type simplifies the approach by treating the solid solution as an ideal solid phase [12,13].

However, it is now evident [14–18] that usually the orthorhombic solid phase is the most important solid crystalline structure for multi-component systems of *n*-paraffins, even if the solid solution is composed only of even alkanes.

From this basis for the nature of the solid phase, the behaviour representation of this diesel has already be

Fig. 1. Melting curve of the diesel: experimental and calculated values.
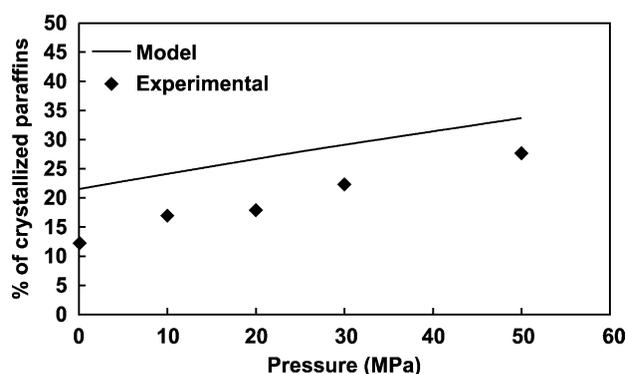

Fig. 2. Percentage of paraffins crystallized in the diesel versus the pressure at 263.15 K: experimental and calculated values.
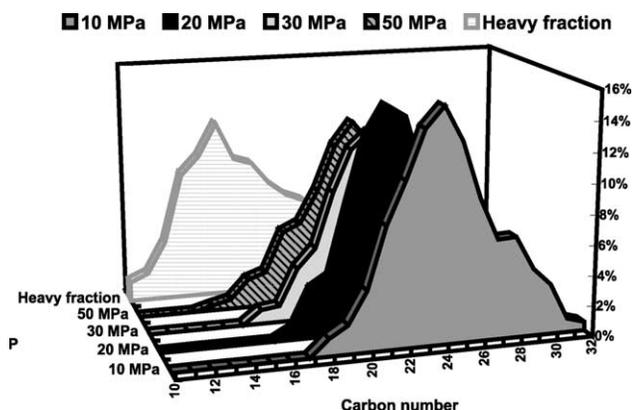
Fig. 3. 3D diagram of the evolution of the solid phase composition versus the pressure at 263.15 K.

presented in a previous work [1]. This approach which used two different excess Gibbs energy models to describe the non-ideality of both solid and liquid phases at atmospheric pressure leads to an accurate description of solid–liquid equilibrium for synthetic mixtures as well as for real systems such as this diesel.

From the foundations of this model, a procedure for the prediction of fluid–solid equilibrium of light gases–heavy hydrocarbons systems under pressure was successfully developed and applied to binary mixtures and multi-components synthetic systems [4] and recently to real petroleum fluids [19].

The description of solid–liquid phase equilibrium under pressure is based on the equality of the fugacities of individual components in all phases:

$$f_i^V(T,P,x_i^V) = f_i^L(T,P,x_i^L) = f_i^S(T,P,x_i^S), \qquad i = 1,2,...,N$$

By assuming the liquid phase as the reference phase r, the equilibrium equation can be rewritten in terms of equilibrium ratios K_i^V and K_i^S :

$$K_i^V = \frac{\phi_i^L}{\phi_i^V}$$

$$K_i^S = \frac{\phi_i^L}{\gamma_i^S \phi_i^{S_0}}$$

in which the fugacities in the fluid phases are expressed in terms of the fugacity coefficients, ϕ_i^V and ϕ_i^L, whereas the fugacity of the solid, considered as a single solid solution made up of all the paraffinic components of the heavy fraction, is described by an activity coefficient γ_i^s.

3.1. Fluid phases modelling

Evaluation of liquid and vapor fugacity coefficients under high pressure requires the use of an equation of state (EOS). It is then possible for mixtures to associate the EOS to the classical quadratic mixing rules which will provide a good description of the fluid phase equilibria. This in spite of the errors on the fugacities of both gas and liquid phases that are

compensated by the equilibrium ratio. In the case where one or more solid phases have to be considered leading to a fluid–fluid–solid(s) equilibrium, a gamma–phi approach must be used and the error compensation no longer takes place between the solid and fluid phases and a significant deviation in the description of the phase equilibrium is noticed. Since the non-ideality of liquid solutions made up of asymmetric components is well described with an excess Gibbs energy model at atmospheric pressure [20,21], a mixing rule which combines an EOS with a G^E expression is used to describe the fugacity in the fluid phases. The EOS/G^E mixing rule concept, which was first introduced by Huron and Vidal [22] consists in replacing the classical quadratic mixing rule of the attractive term of a cubic EOS by an expression which derives from the G^E model at a reference pressure. Among the various EOS/GE mixing rules available the LCVM [23] was chosen because it yields a good prediction of high-pressure vapor–liquid equilibrium of asymmetric light/heavy hydrocarbons systems [24]. Due to the superior description of the pure compounds fugacities the EOS SRK corrected by the volume translation of Peneloux [25] was used with LCVM [26]:

$$P = \frac{RT}{(V'-b)} - \frac{a(T)}{V'(V'+b)} \qquad \text{with } V = V' + C$$

For mixtures, the conventional mixing rule is kept for the parameter b whereas the coefficient a is related to the excess Gibbs free energy according to the following relation:

$$\alpha = \left(\frac{a}{bRT}\right) = \left(\frac{\lambda}{A_v} + \frac{1-\lambda}{A_m}\right)\left(\frac{G^E}{RT}\right) + \frac{1-\lambda}{A_m}\sum_i x_i \ln\left(\frac{b}{b_i}\right) + \sum_i x_i \alpha_i$$

where A_m, A_v and λ are constants. The excess Gibbs free energy G^E of the liquid mixture is calculated using the original UNIFAC group contribution method [27].

3.2. Solid phase modelling

In a process at constant temperature the variation in the fugacity with pressure can be evaluated by integration of the solid molar volume:

$$\ln f_i^S(P) = \ln f_i^S(P_0) + \frac{1}{RT}\int_{P_0}^{P} \bar{V}_i^S \, dP$$

which according to Schaerer [28] may be taken as proportional to the subcooled liquid molar volume:

$$V_i^{S_0} = \bar{\beta} V_i^{L_0}$$

where the value of proportionality coefficient $\bar{\beta}$ assumed pressure independent for each paraffin ranging between C_{15} and C_{40} The value of $\bar{\beta}$ is 0.855 for pure n-alkanes but as shown previously [4] if a value of 0.9 is used for complex systems it takes into account the excess volume of the mixture.

The challenge for the description of the solid fugacity under is to take into account the non-ideality of the orthorhombic phase which can be well represented by an activity coefficient model as it was previously shown at atmospheric pressure [21]. Therefore, the solid fugacity at reference pressure P_0 can be expressed in terms of activity coefficients at atmospheric pressure by

$$f_i^S(P_0) = x_i^S \gamma_i^S(P_0) f_i^{S_0}(P_0)$$

where the fugacity of the pure solid at the same pressure and temperature has to be determined. The fugacity $f_i^{S_0}(P_0)$ can be related to the pure subcooled liquid fugacity $f_i^{L_0}(P_0)$ from the change of free energy between the pure solid and the liquid at temperature T [29]. Assuming that the contribution of specific heat is negligible the change of free energy can be expressed by

$$\ln\frac{f_i^{S_0}(P_0)}{f_i^{L_0}(P_0)} = -\frac{\Delta G^{SL_0}}{RT}$$

$$= -\frac{\Delta H^{SL_0}}{RT}\left(1 - \frac{T}{T^m}\right) - \frac{\Delta H^{tr}}{RT}\left(1 - \frac{T}{T^{tr}}\right)$$

where T^m is the melting temperature and ΔH^{SL_0} the enthalpy of fusion whereas T^{tr} is the transition temperature and ΔH^{tr} the enthalpy of solid–solid transitions. When the last equations are combined the fugacity coefficient of the pure solid at reference pressure cancels out and the solid fugacity coefficient becomes

$$f_i^S(P) = x_i^S \gamma_i^S(P_0)(f_i^{L_0}(P_0))^{1-\beta}(f_i^{L_0}(P))^{\beta}$$

$$\exp\left\{-\frac{\Delta H^{SL_0}}{RT}\left(1 - \frac{T}{T^m}\right) - \frac{\Delta H^{tr}}{RT}\left(1 - \frac{T}{T^{tr}}\right)\right\}$$

leading to the solid–liquid equilibrium ratio:

$$K_i^S = \frac{\phi_i^L(P)(\phi_i^{L_0}(P_0))^{\beta-1}(\phi_i^{L_0}(P))^{-\beta}}{\gamma_i^S(P_0)}\left(\frac{P}{P_0}\right)^{1-\beta}$$

$$\exp\left\{\frac{\Delta H^{SL_0}}{RT}\left(1 - \frac{T}{T^m}\right) + \frac{\Delta H^{tr}}{RT}\left(1 - \frac{T}{T^{tr}}\right)\right\}$$

The activity coefficient which represents the deviation from the ideal behaviour of the solid phase is determined from a modified [21] equation of Wilson [30].

It must be stressed that the equilibrium ratio K_i^S is calculated only from liquid fugacity (pure and partial) coefficients and from pure phase transition properties at reference pressure whereas the liquid fugacity coefficients are calculated from the LCVM, and the pure thermophysical properties come from the literature data leading to a complete predictive description of wax formation in the diesel.

3.3. Prediction

The information from Table 1 are used to characterize the aromatics and the saturated non-crystallizable
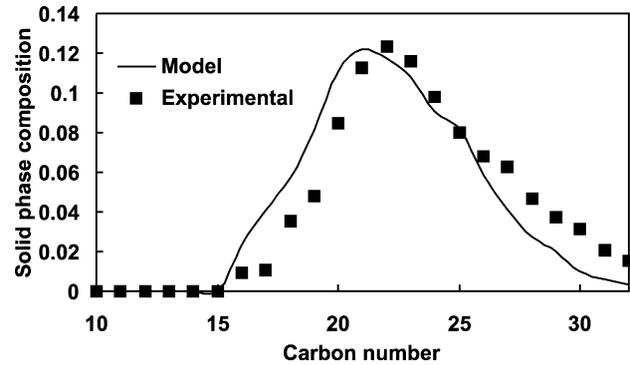

Fig. 4. Predicted and experimental solid phase composition at 30 MPa and 263.15 K.

(naphthenic and branched alkanes) pseudo-compounds. Hexylbenzene is used for aromatics and trimethyltride-cane for the saturated non-crystallizable compounds in order to reproduce the average molecular weight of the diesel [1].

As shown in Fig. 1 there is an excellent agreement between experimental and calculated value demonstrating that the influence of the pressure on the wax disappearance temperature is well described qualitatively and quantitatively.

As demonstrated in Fig. 2 the model overpredicts the fraction of crystallized paraffins with pressure. Yet there is no increase in the deviations with the pressure. This behaviour has been already observed for other complex fluids [31]. This indicates that the problem with the model is not on the pressure dependence but on the relation between the fugacities of the fluid and solid phases. Since results from a previous work at atmospheric pressure [1] show that the solid phase model can provide a good description of the solid phase behaviour these results seem to indicate that the model used underestimates the non-ideality of the fluid phases.

The comparison of both experimental and calculated solid phase composition can be found in Figs. 4 and 5.
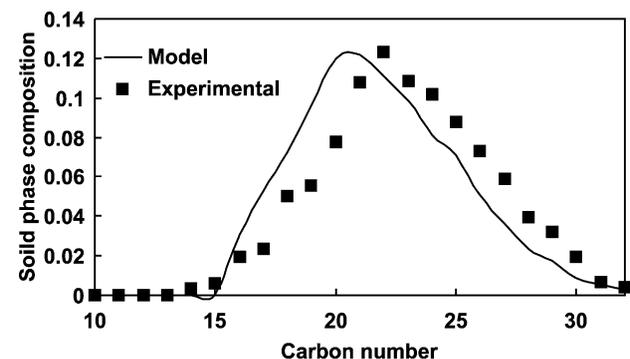

Fig. 5. Predicted and experimental solid phase composition at 50 MPa and 263.15 K.
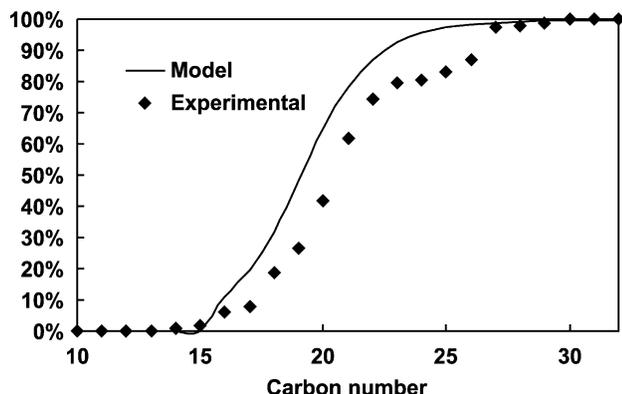
Fig. 6. Predicted and experimental % of crystallization for each paraffin of the diesel at 50 MPa and 263.15 K.

Again the influence of the pressure on the paraffin behaviour is well described but these results do not provide an explanation for the overprediction of the solid deposit data.

For the purpose of understanding the model limitations it is more revealing to represent the percentage of crystallization of each paraffins at 50 MPa as shown in Fig. 6. These results indicate that the approach used overestimates the crystallization of the intermediate *n*-alkanes (Table 4). Since for this fluid they represent the majority of the components, this leads to an overestimation of the solid deposit.

4. Conclusion

The influence of the pressure on the precipitation of the heavy molecules in a diesel has been studied in this work. Two different apparatus have been employed to determine accurately the wax disappearance temperatures up to 100 MPa and the solid phase amount and composition at a temperature of 263.15 K up to 50 MPa. The results obtained show an increase in the diesel cloud point of about 25 °C at the operating pressure of a common rail engine. It is clear from our results that the increase of the diesel cloud point must be taken into account in the development of new diesel engines where the diesel is injected under high pressure.

The model used can provide an excellent description of the melting point of the diesel on the whole range of pressure. The behaviour below the cloud point is also well described but an overestimation of solid phase quantity versus the pressure is obtained.

Table 4
Percentage of crystallization for each paraffin of the diesel at 263.15 K vs pressure

	P (MPa)			
	10	20	30	50
C10	0.00	0.00	0.00	0.00
C11	0.00	0.00	0.00	0.00
C12	0.00	0.00	0.00	0.00
C13	0.00	0.00	0.00	0.00
C14	0.00	0.00	0.00	0.85
C15	0.00	0.00	0.00	1.74
C16	0.00	0.00	2.47	6.17
C17	0.00	1.33	2.76	7.66
C18	2.61	7.36	10.58	18.49
C19	5.52	11.88	18.09	26.66
C20	13.00	26.54	33.00	41.81
C21	29.75	46.36	50.63	61.84
C22	45.38	63.58	65.67	74.44
C23	60.41	72.37	73.85	79.41
C24	70.86	73.98	77.59	80.23
C25	71.17	74.46	78.39	83.02
C26	73.25	77.83	78.19	86.89
C27	75.59	85.55	85.65	97.54
C28	86.08	87.43	88.05	97.80
C29	82.40	84.75	88.68	98.79
C30	86.69	100.00	100.00	100.00
C31	100.00	100.00	100.00	100.00
C32	100.00	100.00	100.00	100.00

References

[1] Coutinho JAP, Dauphin C, Daridon JL. Fuel 2000;79:607–16.
[2] Daridon JL, Pauly J. Phys Chem Chem Phys 2002;4:4458–61.
[3] Daridon JL, Dauphin C. Meas Sci Technol 1999;10:1309.
[4] Pauly J, Daridon JL, Coutinho JAP, Lindeloff N, Andersen SI. Fluid Phase Equilib 2000;167:145–59.
[5] Monger-McClure TG, Tackett JE, Merril LS. SPE Prod Facilities 1999;14(1).
[6] Pauly J, Daridon JL. Fluid Phase Equilib 2001;187/188:71–82.
[7] Durand JP, Fafet A, Barreau A. J High Resolut Chromatogr 1989;12: 230.
[8] Daridon JL, Xans P, Montel F. Fluid Phase Equilib 1996;17:241–8.
[9] Rønningsen HP, Sømme BF, Pedersen KS. Proceedings from Multiphase '97, BHR Group; 1997.
[10] Ruffier-Méray V, Brucy F, Béhar E. Proceedings from Multiphase '97, BHR Group; 1997.
[11] Ungerer P. Fluid Phase Equilib 1995;111:287–311.
[12] Erickson DD, Niesen VG, Brown TS. SPE 1993;22604:933–48.
[13] Hansen JH, Fredenslund Aa, Pedersen KS, Rønningsen HP. AICHE J 1988;12:1937–42.
[14] Dirand M, Chevallier V, Provost E, Bouroukba M, Petitjean D. Fuel 1998;77(12):1253–60.
[15] Chevallier V, Provost E, Bourdet JB, Bouroukba M, Petitjean D, Dirand M. Polymer 1999;40:2121–8.
[16] Chevallier V, Petitjean D, Bouroukba M, Dirand M. Polymer 1999;40: 2129–37.
[17] Craig SR, Hastie GP, Roberts KJ, Gerson AR, Sherwood JN, Tack RD. J Mater Chem 1998;8:859–69.
[18] Gerson AR, Roberts KJ, Sherwood JN. Am Inst Chem Engng Symp Ser 1991;284:138–42.
[19] Daridon JL, Pauly J. Energy Fuels 2001;15:730–5.

[20] Coutinho JAP, Andersen SI, Stenby EH. Fluid Phase Equilib 1995; 103:23.

[21] Coutinho JAP, Knudsen K, Andersen SI, Stenby EH. Chem Engng Sci 1996;51:3273.

[22] Huron MJ, Vidal J. Fluid Phase Equilib 1979;3:255–71.

[23] Boukouvalas CJ, Spiliotis N, Coustikos Ph, Tzouvaras N, Tassios DP. Fluid Phase Equilib 1994;92:75.

[24] Boukouvalas CJ, Magoulas KG, Stamataki SK, Tassios D. Ind Engng Chem Res 1997;36:5454.

[25] Peneloux A, Rauzy E, Frèze R. Fluid Phase Equilib 1982;8: 7–23.

[26] Hartono R, Mansoori GA, Suwono A. Chem Engng Commun 1999; 23:173.

[27] Fredenslund A, Gmehling J, Rasmussen P, Amsterdam: Elsevier; 1977.

[28] Schaerer AA, Busso CJ, Smith AE, Skinner LB. J Am Chem Soc 1986;77:2017.

[29] Prausnitz JM. Molecular thermodynamics of fluid phase equilibria. Englewood Cliffs, NJ: Prentice-Hall; 1969.

[30] Wilson GM. J Am Chem Soc 1964;86:127.

[31] Pauly J, Dauphin C, Daridon JL, Coutinho JAP. XXVI JEEP, March 2000.